Thermal calcium atom interferometer with a phase resolution of a few milliradians based on a narrow-linewidth diode laser

Tomoya Akatsuka, Yoshihiro Mori, Nobuhiko Sone, Yurie Ohtake, Mamoru Machiya, and Atsuo Morinaga
Faculty of Science and Technology, Tokyo University of Science, Noda-shi, Chiba 278-8510, Japan
(Received 27 May 2011; published 25 August 2011)

A symmetrical atom interferometer with a thermal calcium atom beam has been developed using a narrow linewidth diode laser stabilized to the resonance of a high-finesse cavity. The linewidth of the diode laser was estimated to be less than 1 Hz relative to the cavity resonance in noise measurement over the range of 100 Hz to 1 MHz, and the phase instability of the interference fringes obtained from the Allan deviation was improved to 2 mrad at an integration time of 300 s. Using this atom interferometer, the ac Stark phase shift between the $^1S_0$ and $^3P_1$ states of a Ca atom was measured as a function of a laser power near the resonance of the $^1S_0$-$^1P_1$ transition at a wavelength of 423 nm. The decay rate of the $^1P_1$ state was determined to be $\gamma = 1.91(33) \times 10^8\ \mathrm{s}^{-1}$.

DOI: 10.1103/PhysRevA.84.023633 PACS number(s): 03.75.Dg, 32.60.+i, 37.25.+k, 42.60.By

I. INTRODUCTION

Atom interferometers have been developed as sensitive detectors for precision measurements and for fundamental tests in quantum physics, because of their phase sensitivity and wide range of applications owing to their mass and internal structure, which are different from those of electron, neutron, and photon interferometers [1]. In particular, optical Ramsey-Bordé atom interferometers employing beam splitters and deflectors based on a resonant one-photon process are powerful tools for precise frequency and phase measurements in modern science [2]. These interferometers can be classified into symmetrical and asymmetrical configurations [3–5]. Optical Ramsey-Bordé atom interferometers were first developed in the space domain using thermal atomic beams [6]. Subsequently, those in the time domain using laser-cooled atoms and light pulses have been developed [7] and are commonly used for various applications, because the interrogation time of the atom in the interferometer can be markedly increased [8]. However, to measure the phase shift of particles moving in the vector potential, such as the shift due to the Aharonov-Casher effect [9] and the Röntgen effect [10], atom interferometers in the space domain are still necessary.

Interferometers with asymmetrical configurations require two pairs of counterpropagating running waves and enclose trapezoidal areas. Such interferometers are sensitive to the frequency detuning of lasers; therefore, they have been used in several methods of high-precision spectroscopy of narrow atomic lines to realize optical clocks because of their advantages over single-pulse (Rabi) spectroscopy [11]. In optical clock experiments, the frequency of the laser interrogating the clock transition is locked to the center of the Ramsey fringe under the condition that the external perturbations that cause a frequency shift of the resonance are carefully suppressed [12]. However, in terms of measuring the quantum phases induced on atoms, the phase resolution of the Ramsey-Bordé atom interferometer is limited by frequency fluctuations of the laser over a long integration time. On the other hand, symmetrical configurations comprised of four copropagating running waves enclose parallelogram-shaped areas [4]. The phase of interference fringes, in principle, depends on the laser phase difference $\Delta\phi_\mathrm{L} = -\phi_1 + \phi_2 + \phi_3 - \phi_4$, where ϕ_i is the laser phase of the ith running wave, adding to the perturbation phase. Therefore, interferometers with symmetrical configurations are far less sensitive to frequency fluctuations of the laser and act as white-light interferometers.

Previously, our group developed a symmetrical atom interferometer based on the $^1S_0$-$^3P_1(m_J = 0)$ transition of Ca at 657 nm [13]. We obtained interference fringes with a visibility of about 0.15 for an interval of 8 mm between the first and second laser beams. The visibility of the interference fringes decreased as the beam interval increased. The phase fluctuation of the fringes was about 300 mrad and was independent of the integration time. A laser system with a linewidth of tens of kilohertz was used. The most probable velocity of the atomic beam was about 800 m/s, so that the atoms needed 10 μs from the first laser beam to the second one. It led to a frequency fluctuation of 5 kHz while an atom was in the interaction region. It is necessary to suppress the fluctuation of the laser phase $\Delta\phi_\mathrm{L}$ while an atom interacts with four laser beams, in order to obtain a higher phase resolution and detect small perturbations. For example, a laser system with a frequency fluctuation of 16 Hz in 10 μs will be required to achieve a phase resolution of less than 1 mrad, even if a symmetrical atom interferometer is used.

In this paper we present the performances of a symmetrical atom interferometer based on a narrow-linewidth diode laser. First, we describe our diode laser system, which is stabilized to the resonance of a high-finesse cavity isolated from acoustic and vibrational noise and heat conduction to suppress the phase fluctuation. Next, we evaluate the phase stability of the interference fringes and the linewidth of the laser by measuring the Allan deviation. Finally, we use the atom interferometer to measure the ac Stark phase shift on the $^1S_0$-$^3P_1(m_J = 0)$ transition by applying a laser power near the resonance of the $^1S_0$-$^1P_1$ transition at 423 nm (see Fig. 1). The decay rate of the $^1P_1$ state was obtained from the ac Stark phase shift.

II. EXPERIMENTAL SETUP

A schematic of the experimental setup is shown in Fig. 2. The laser system, which operated at 657 nm, was based

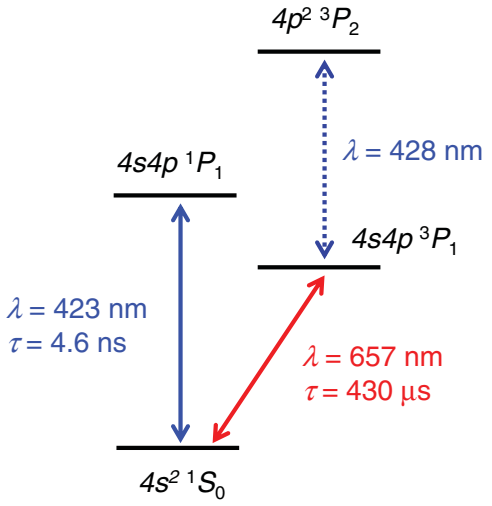

FIG. 1. (Color online) Partial energy level diagram of ^{40}Ca. λ, resonant wavelength; τ, lifetime.

on an external cavity diode laser (ECDL) consisting of an antireflection(AR)-coated diode laser, a holographic diffraction grating of 1800 lines/mm, and a mirror mounted on a piezoelectric transducer (PZT), which formed a 12-cm-long extended cavity in the Littman configuration for the first-order diffracted beam. The typical output power of the ECDL was 3 mW at a diode laser current of 62 mA. Part of the laser output was frequency tuned by a double-pass acousto-optic modulator (AOM) and transferred to a reference cavity via a 10-m-long polarization maintaining (PM) single-mode optical fiber. The reference cavity consisted of two ultralow-expansion (ULE) glass mirrors optically contacted on a 10-cm-long cylindrical ULE glass spacer. The cavity finesse was determined to be 3.8×10^5 by the cavity ring-down method, which corresponds to a cavity full-resonance linewidth of 3.9 kHz. The cavity was housed in double aluminum radiation shields placed in a vacuum chamber to maintain a stable cavity temperature. To isolate the cavity from acoustic and vibrational noise and heat conduction, the cavity and the inner radiation shield were supported by small elastomer (Viton) pieces, and the vacuum chamber was mounted on a vibration-isolation table with a resonance frequency of 0.5 Hz enclosed in a soundproof box. The transferred laser via the optical fiber was phase-modulated at 15 MHz by an electro-optic modulator (EOM) and coupled to the reference cavity. The error signal obtained by the Pound-Drever-Hall (PDH) method [14] was fed back to the diode laser current and the PZT to stabilize the laser frequency to a resonance of the cavity. According to an estimation of the intensity noise of the reflected light of the cavity, the frequency fluctuation of the stabilized laser was 500 Hz over the range of 100 Hz to 1 MHz. Assuming the white frequency noise in this regime, the laser linewidth was estimated to be 0.8 Hz relative to the cavity resonance [15]. To obtain a more reliable estimation of the laser phase stability, optical beat measurement with another laser with a comparable linewidth is in progress.

A Ramsey-Bordé atom interferometer with a symmetrical configuration was realized on a thermal calcium atom beam interacting with four copropagating laser beams [13]

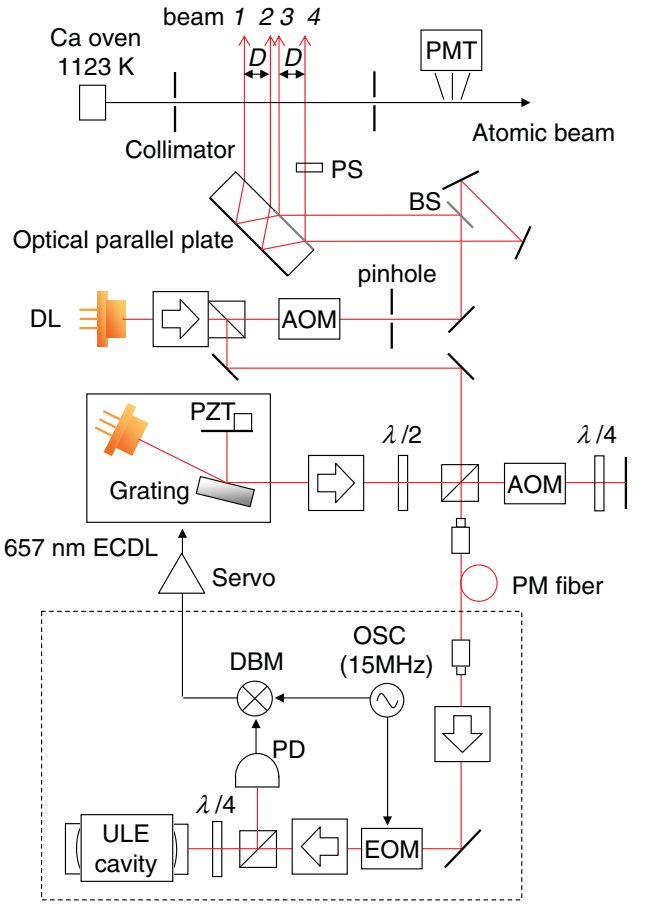

FIG. 2. (Color online) Experimental setup of the thermal calcium atom interferometer based on a diode laser stabilized to a reference cavity by the Pound-Drever-Hall method. DL, diode laser; ECDL, external cavity diode laser; PZT, piezoelectric transducer; AOM, acousto-optic modulator; EOM, electro-optic modulator; OSC, RF oscillator; DBM, double balanced mixer; PD, photo diode; BS, beam splitter; PS, phase shifter; and PMT, photomultiplier tube.

perpendicular to the atomic beam as shown in Fig. 2. An oven at a temperature of 1123 K produced the thermal calcium atom beam with the most probable velocity of 840 m/s, corresponding to a de Broglie wavelength of 8.2 pm, which was collimated by apertures inserted before and after the interaction region. An AR-coated diode laser was injection locked to the ECDL output to amplify the power up to a maximum of 50 mW, which was power-controlled by an additional AOM, mode-cleaned to a nearly perfect Gaussian beam profile by a pinhole of 50 μm diameter, collimated at a beam radius of 0.55 mm, and divided into four copropagating parallel beams by a beam splitter and an optical parallel plate. Then the four beams were introduced into the interaction region perpendicular to the atomic beam. The separation D between laser beams 1 and 2 (3 and 4) depicted in Fig. 2 was tunable from 4 to 16 mm, while that between laser beams 1 and 3 (2 and 4) was fixed to 20 mm; thus the total length of the interaction region was from 24 to 36 mm. The power of each laser beam was adjusted so as to maximize the amplitude of interference fringes. A phase shifter (PS) made of fused silica with a refractive index of 1.4564 at

room temperature was inserted into the path of laser beam 4 to scan the laser phase $\Delta\phi_L$. A magnetic field of 0.48 mT was applied perpendicular to both the atomic beam and the laser beams in the interaction region, which caused the first order Zeeman shifts of ± 10 MHz on the $m_J = \pm 1$ sublevels of the $^3P_1$ state, respectively. The polarization of each laser beam was set parallel to the magnetic field so that atoms were excited to the $m_J = 0$ sublevel. Spontaneous emission from the $^3P_1(m_J = 0)$ excited state to the $^1S_0$ ground state was detected by a photomultiplier tube (PMT) in the detection region with length $l_d = 50$ mm located at $l = 250$ mm downstream from the interaction region. Note that the lifetime $\tau = 430$ μs of the $^3P_1$ state [16] was comparable to the mean time until atoms reached the detection region after interacting with the laser beams; therefore, the velocity distribution of atoms contributing to the interference signal was weighted by the factor $\exp[-l/(v\tau)]\{1 - \exp[-l_d/(v\tau)]\}$. Taking this factor into account, we used $v_a = 830$ m/s as the typical velocity of atoms.

III. MEASUREMENT

A. Phase stability

For the alignment and frequency tuning of the laser beams, we observed the fluorescence spectrum of the $^1S_0$-$^3P_1(m_J = 0)$ transition obtained by a retroreflected laser beam perpendicular to the atomic beam. Figure 3 shows a typical observed spectrum, in which the laser frequency was controlled by tuning the modulation frequency of the double-pass AOM inserted between the ECDL and the reference cavity. The 10 MHz full width at half maximum (FWHM) of the spectrum was Doppler broadening due to the residual transverse velocity of the atomic beam, while the 500 kHz linewidth of the Lamb-dip spectrum was mainly due to the transit time of 2 μs of atoms through the laser intensity distribution. Each laser beam was aligned so that the Lamb-dip spectrum approached the center of the Doppler spectrum, and then the laser frequency was set to the center of the resonance before starting interference measurement.

The laser phase $\Delta\phi_L$ was scanned by periodically sweeping the angle of the phase shifter at 10 Hz, and the interference fringes were observed repeatedly for 40 ms every 100 ms. The

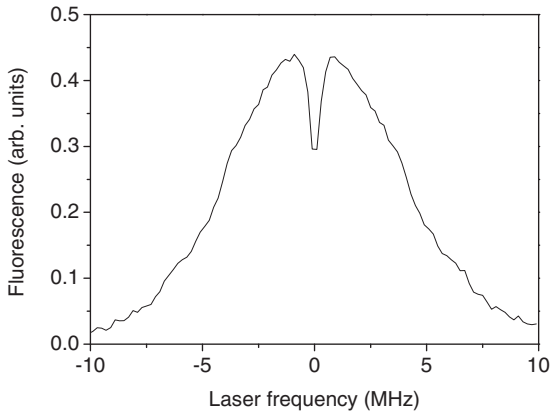

FIG. 3. Typical fluorescence spectrum of the $^1S_0$-$^3P_1(m_J = 0)$ transition of the thermal calcium atom beam excited by a retroreflected laser beam pair.

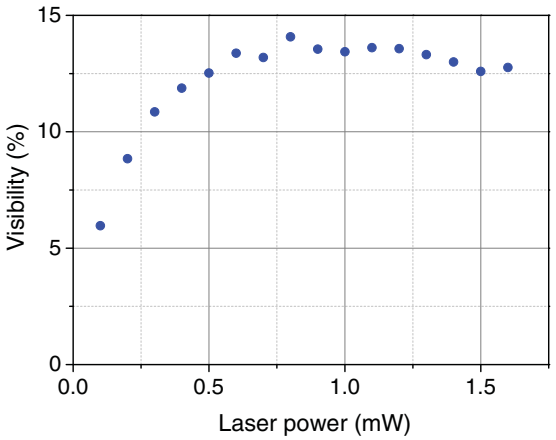

FIG. 4. (Color online) Visibility as a function of the laser power.

visibility of the interference fringes was measured as a function of laser power, as shown in Fig. 4. The visibility reaches a maximum at a laser power exceeding 0.6 mW, which is known as the $\pi/2$ pulse area [17]. Figure 5 shows a typical interference fringe integrated for 80 000 scans under the beam separation of $D = 16$ mm. The laser phase of the x axis was calibrated from the incident angle of the laser beam to the phase shifter. The origin of the x axis corresponds to the incident angle of zero. The center level of the interference fringes fluctuated within 10% of the fringe amplitude during the measurement. This corresponds to the laser power fluctuation of 1% or the oven temperature fluctuation of 1 K, which were consistent with the experimental conditions. The laser power fluctuation around 0.6 mW causes the slight variation of visibility as shown in Fig. 4, and the oven temperature fluctuation does not influence the visibility. For a single scan, the intensity noise of the interference signal was 5%, which was consistent with the photocurrent shot noise of the present condition. The visibility of the observed interference fringe was 0.14, which was in good agreement with the calculation in Ref. [13] upon taking the present residual Doppler linewidth into consideration. The visibility had no noticeable dependence on D, as shown in Fig. 6. This suggests that the fluctuation of the laser phase while atoms passed through the interaction region had disappeared completely.

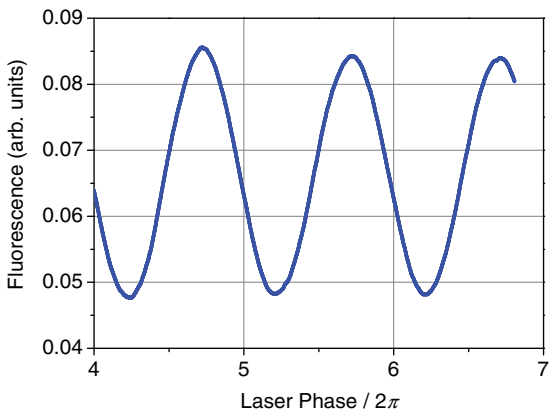

FIG. 5. (Color online) Typical interference fringe integrated for 80 000 scans under the beam separation $D = 16$ mm.

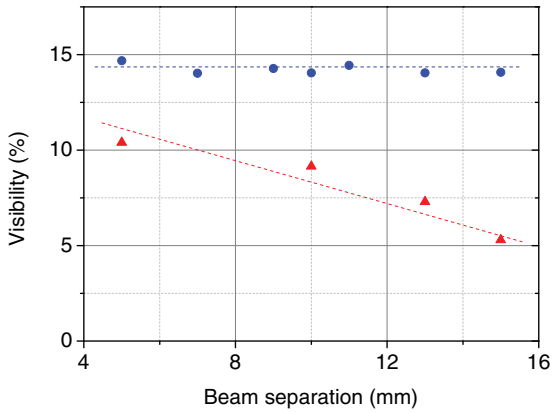

FIG. 6. (Color online) Visibility as a function of the beam separation. ●: Present results.▲ : Results with 10 kHz linewidth laser. The dashed lines are a guide to the eye.

The phase stability of the interference fringe was investigated by calculating the Allan deviation at different integration times. Sequentially observed interference fringes for 40 ms were integrated every 20 scans (the integration time is 0.8 s) and fitted by a sine function $\sin[\Delta\phi_{\mathrm{L}} - \varphi(n)]$ to obtain their phase $\varphi(n)$, where n is the number of the data every 20 scans. A typical fitting uncertainty of $\varphi(n)$ was 7 mrad. Figure 7(a) shows the Allan deviation calculated from the 4000 data set of the interference phase $\varphi(n)$ as a function of the integration time. In the short-term regime, the Allan deviation decreased with increasing integration time because of the improved signal-to-noise ratio. Although it was indicated that the interference fringe had no significant phase noise because the amplitude of the fringe did not decay during integration for 80 000 scans in Fig. 5, the Allan deviation increased in the long-term regime. This is mainly due to the drift of the laser phase $\Delta\phi_{\mathrm{L}}$, which is related to the refractive index of the phase shifter depending on the temperature, which was estimated to be 25 mrad/K. The interference phase $\varphi(n)$ depends on the phase drift linearly because the drift adds only on the ϕ_4. The linear phase drift of $\Delta\phi_{\mathrm{L}}$ increases the Allan deviation linearly with the integration time.

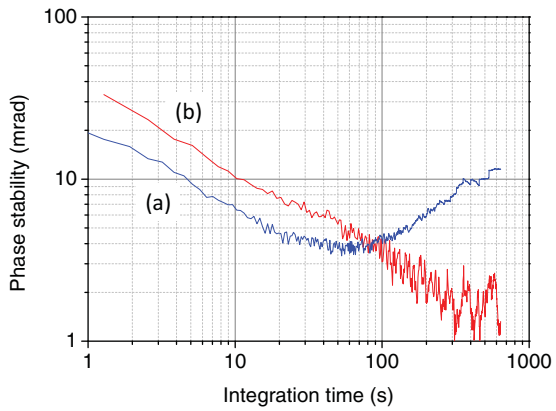

FIG. 7. (Color online) Allan deviation calculated from data sets of (a) the phase $\varphi(n)$ and (b) the differential phase $\varphi(2n) - \varphi(2n-1)$ of the interference fringes as a function of the integration time.

For the detection of an atomic phase shift induced by an applied perturbation, the long-term phase drift can be canceled out by comparing the interference phase with a perturbation with that without a perturbation in a short cycle and integrating the differential phase to improve the signal-to-noise ratio. The Allan deviation calculated from the data set of the differential interference phase $\varphi(2n) - \varphi(2n-1)$ with subsequent integration decreased even in the long-term regime and reached 2 mrad at an integration time of 300 s as shown in Fig. 7(b). The phase stability of 2 mrad corresponds to the frequency fluctuation of 16 Hz of the laser during interaction with an atom. In the longer integration time, the Allan deviation may be limited by the present linear phase drift of 30 μrad during 40 scans, which will be suppressed by stabilizing the temperature of the phase shifter. Simultaneously, the influence of the frequency fluctuation of the laser and the differential refractive index of air on the paths of four laser beams may be the limitation of the phase resolution. In future experiments, suppressing the photocurrent shot noise by increasing the atomic beam flux and optimizing the detection of the fluorescence will allow us to investigate the phase stability of the submilliradian range at the integration time of 100 s.

B. ac Stark phase shift

Using the present atom interferometer, the ac Stark phase shifts of the $^1S_0$-$^3P_1$ line of the Ca atom were measured for a perturbing laser wavelength of 423 nm near the resonance of the $^1S_0$-$^1P_1$ transition. Previously, the phase shifts due to the ac Stark effect were investigated using asymmetrical atom interferometers of Mg and Ca atoms; however, there was no successful quantitative comparison with the decay rate [18–20].

The ac Stark phase shift induced on atoms moving with velocity v_a in the ac Stark potential U of the perturbing laser is given by

$$\varphi_{\mathrm{ac}} = -\frac{1}{\hbar}\int U\,dt = \frac{1}{\hbar v_a}\int \frac{\alpha I}{2\varepsilon_0 c}dx, \tag{1}$$

where α is the electric dipole polarizability of atoms, which depends on the laser frequency, laser polarization, and atomic state; I is the local laser intensity; ε_0 is the electric constant; and c is the speed of light in vacuum. When the perturbing laser has a Gaussian beam profile with a beam radius of w, the phase shift of the interference fringe is given by

$$\Delta\varphi_{\mathrm{ac}} = \frac{\alpha(^3P_1) - \alpha(^1S_0)}{\sqrt{2\pi}\hbar\varepsilon_0 c w v_a}P, \tag{2}$$

where P is power of the perturbing laser. The electric dipole polarizability α of atoms in a specific state for laser frequency ω is generally described as the summation of the contributions from all dipole transitions between the state and upper states k with respective decay rates γ_k, Clebsch-Gordan coefficients c_k, and transition frequencies ω_k:

$$\alpha = 6\pi\epsilon_0 c^3 \sum_k \frac{c_k^2\gamma_k}{\omega_k^2\left(\omega_k^2 - \omega^2\right)}. \tag{3}$$

If the perturbing laser is tuned to the resonance frequency ω_0 of the $^1S_0$-$^1P_1$ transition with detuning $\Delta = \omega - \omega_0$ (Under

this condition, the contributions of the other transitions from both the ground $^1S_0$ and excited $^3P_1(m_J = 0)$ states, the largest of which is from the $4s4p^3P_1 - 4p^2\,^3P_2$ transition at 428.423(1) nm, are 10^{-3} times less than that of the 423 nm transition, and the counterrotating term is also negligible [21].), then the polarizability of atoms in the ground state is described as

$$\alpha(^1S_0) = -\frac{3\pi\varepsilon_0 c^3\gamma}{\omega_0^3}\frac{1}{\Delta}, \tag{4}$$

where the decay rate $\gamma = 2.15(2) \times 10^8$ s^{-1} of the 423 nm transition is precisely determined from photoassociation spectroscopy [22].

The perturbing laser was based on an infrared laser system consisting of an ECDL at 846 nm as the master oscillator, an isolator, and a tapered amplifier. The blue light at 423 nm was generated by second harmonic generation (SHG) using a periodically poled $KTiOPO_4$ (KTP) crystal placed in a laboratory-built bow-tie optical cavity. The laser frequency was determined by saturated absorption spectroscopy of the $^1S_0$-$^1P_1$ transition of Ca atoms in a discharge cell. The power of the output laser was controlled by an AOM, mode cleaned by a pinhole, collimated at a beam radius of $w = 1.2$ mm, and incident perpendicular to the atomic beam with its polarization parallel to the magnetic field. The perturbation region was between the 657 nm laser beams 1 and 2, where atoms were in the superposition state of $^1S_0$ and $^3P_1(m_J = 0)$. The beam radius w of the perturbing laser was about twice as large as that of the 657 nm laser beams; thus, we assumed that atoms contributing to the interference fringe passed through the center of the Gaussian intensity distribution of the perturbing laser.

In the phase measurement sequence, the interference fringes with and without the perturbing laser were recorded at odd and even n, respectively. Typical interference fringes integrated at $n = 80$ for several powers of the perturbing laser at detuning $\Delta/(2\pi) = 1.6$ GHz are shown in Fig. 8. With the increase in the power of the perturbing laser, the phase was clearly shifted, while the amplitude of the fringes decreased with increasing phase shift owing to their dispersive features.

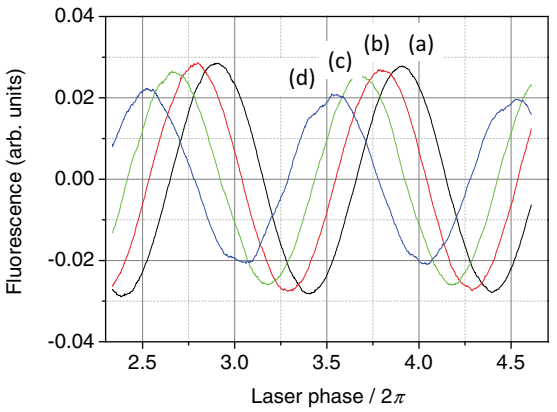

FIG. 8. (Color online) Interference fringes with the ac Stark shift for the perturbing laser power of (a) 0.0, (b) 1.0, (c) 2.1, and (d) 3.5 mW.

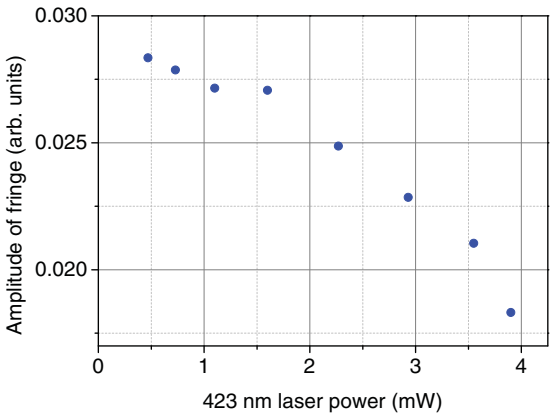

FIG. 9. (Color online) Amplitude of the interference fringes as a function of the perturbing laser power.

Figure 9 shows the amplitude of the fringes as a function of the power of the perturbing laser.

Figure 10 shows the phase shift of the interference fringe as a function of the power P of the perturbing laser at detuning of $\Delta/(2\pi) = 1.6$ GHz. The obtained power dependence of the phase shift was 690(6) rad/W. From Eqs. (2) and (4), the decay rate was derived to be $\gamma = 1.91(33) \times 10^8$ s^{-1} which included systematic uncertainties estimated as follows. The power fluctuation of the perturbing laser was included in the error bar of each datum in Fig. 10 as the fluctuation of the phase shift. The uncertainty of the detuning of the perturbing laser was less than 100 MHz and was due to the uncertainty of the set point before each measurement and the frequency drift during the integration. The beam radius $w = 1.2$ mm of the perturbing laser was measured by a beam profiler with an uncertainty of 0.1 mm. We assumed 10% uncertainty for the velocity $v_a = 830$ m/s of atoms contributing to the interference fringe, which is the typical value for the velocity distribution of a thermal atom beam as described in Sec. II. The value of γ determined from this measurement was in agreement with the known value within an uncertainty.

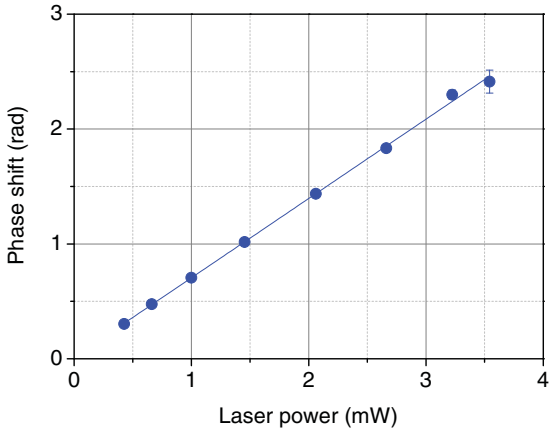

FIG. 10. (Color online) Phase shift of the interference fringe as a function of the power of the perturbing laser at detuning of 1.6 GHz. Error bar of each plot corresponds to the Allan deviation of the data set measured for $n = 80$.

Thus, we could measure the ac Stark phase shift as a function of the power of the perturbing laser with an uncertainty of 1%, although the decay rate γ was deduced with an uncertainty of 17% due to the large uncertainties of thermal atomic velocity and the laser beam radius. Therefore, this atom interferometer will be useful to measure the nondispersive effect; the phase shift does not depend on the velocity of each atom. We are attempting to use the present atom interferometer based on the $^1S_0$-$^3P_1(m_J = 0)$ transition of Ca to verify the nondispersive Röntgen effect [10], whose phase shift is estimated to be about 5 mrad, when the dc voltage of 20 kV/cm and the magnetic field of 20 mT are applied for a 10 mm length in the interrogation zone of the interferometer [23].

IV. CONCLUSIONS

In conclusion, we developed a symmetrical atom interferometer in space domain based on a narrow-linewidth diode laser. The diode laser was stabilized to the resonance of a high-finesse cavity by using the Pound-Drever-Hall method and its linewidth was evaluated at less than 1 Hz relative to the cavity resonance in noise measurement over the range of 100 Hz to 1 MHz. The visibility of interference fringes had no noticeable dependence on the beam separation till 16 mm. From the Allan deviation, the phase stability of the atom interferometer was evaluated to be 2 mrad at an integration time of 300 s.

Using this atom interferometer, the ac Stark phase shifts of the $^1S_0$-$^3P_1(m_J = 0)$ line of the Ca atom were measured for a perturbing laser wavelength of 423 nm near the resonance of the $^1S_0$-$^1P_1$ transition. We could measure the ac Stark phase shift as a function of the power of the perturbing laser with an uncertainty of 1% and the decay rate was derived to be $\gamma = 1.91(33) \times 10^8\ \mathrm{s}^{-1}$, which was in agreement with the known value within an uncertainty. Using the atom interferometer developed in the present experiment, we are now trying to verify the Röntgen effect which is not yet observed experimentally.

ACKNOWLEDGMENT

This research was partially supported by Grant-in-Aid for Scientific Research on Innovative Areas "Extreme quantum world opened up by atoms" (Grant No. 21104006) from the Ministry of Education, Culture, Sports, Science, and Technology, Japan.

[1] A. D. Cronin, J. Schmiedmayer, and D. E. Pritchard, Rev. Mod. Phys. **81**, 1051 (2009).
[2] Ch. J. Bordé, Phys. Lett. A **140**, 10 (1989).
[3] Ch. J. Bordé, in *Laser Spectroscopy*, edited by M. Ducloy *et al.* (World Scientific, Singapore, 1992), p. 239.
[4] A. Morinaga and Y. Ohuchi, Phys. Rev. A **51**, R1746 (1995).
[5] T. Trebst, T. Binnewies, J. Helmcke, and F. Riehle, IEEE Trans. Instrum. Meas. **50**, 535 (2001).
[6] F. Riehle, Th. Kisters, A. Witte, J. Helmcke, and Ch. J. Bordé, Phys. Rev. Lett. **67**, 177 (1991).
[7] K. Sengstock, U. Sterr, G. Hennig, D. Bettermann, J. H. Müller, and W. Ertmer, Opt. Commun. **103**, 73 (1993).
[8] C. W. Oates, F. Bondu, R. W. Fox, and L. Hollberg, Eur. Phys. J. D **7**, 449 (1999).
[9] Y. Aharonov and A. Casher, Phys. Rev. Lett. **53**, 319 (1984).
[10] H. Wei, R. Han, and X. Wei, Phys. Rev. Lett. **75**, 2071 (1995).
[11] V. I. Yudin, A. V. Taichenachev, C. W. Oates, Z. W. Barber, N. D. Lemke, A. D. Ludlow, U. Sterr, Ch. Lisdat, and F. Riehle, Phys. Rev. A **82**, 011804(R) (2010).
[12] C. Degenhardt, H. Stoehr, Ch. Lisdat, G. Wilpers, H. Schnatz, B. Lipphardt, T. Nazarova, P-E Pottie, U. Sterr, J. Helmcke, and F. Riehle, Phys. Rev. A **72**, 062111 (2005).
[13] S. Yanagimachi, Y. Omi, and A. Morinaga, Phys. Rev. A **57**, 3830 (1998).
[14] R. W. P. Drever, J. L. Hall, F. V. Kowalski, J. Hough, G. M. Ford, A. J. Munley, and H. Ward, Appl. Phys. B: Photophys. Laser Chem. **31**, 97 (1983).
[15] D. S. Elliott, R. Roy, and S. J. Smith, Phys. Rev. A **26**, 12 (1982).
[16] S. Kraft, F. Vogt, O. Appel, F. Riehle, and U. Sterr, Phys. Rev. Lett **103**, 130401 (2009).
[17] F. Riehle, A. Morinaga, J. Ishikawa, T. Kurosu, and N. Ito, Jpn. J. Appl. Phys. **31**, L1542 (1992).
[18] F. Riehle, A. Witte, Th. Kisters, and J. Helmcke, Appl. Phys. B **54**, 333 (1992).
[19] U. Sterr, K. Sengstock, J. H. Müller, D. Bettermann, and W. Ertmer, Appl. Phys. B **54**, 341 (1992).
[20] A. Morinaga, T. Tako, and N. Ito, Phys. Rev. A **48**, 1364 (1993).
[21] C. Degenhardt, H. Stoehr, U. Sterr, F. Riehle, and Ch. Lisdat, Phys. Rev. A **70**, 023414 (2004).
[22] C. Degenhardt, T. Binnewies, G. Wilpers, U. Sterr, F. Riehle, Ch. Lisdat, and E. Tiemann, Phys. Rev. A **67**, 043408 (2003).
[23] K. Honda, J. Itimura, N. Sone, and A. Morinaga, in *Book of Abstracts for the 20th International Conference on Atomic Physics* (ICAP 2006, Innsbruck, 2006), p. 244.